Acta Biochim Biophys Sin 2024, 56(4): 607–620
https://doi.org/10.3724/abbs.2024020
Advance Access Publication Date: 26 February 2024
Original Article

Original Article

miR-29b-1-5p exacerbates myocardial injury induced by sepsis in a mouse model by targeting TERF2

Yaqing Jiang[1], Junmei Xu[1], Hua Zeng[1], Zhaojing Lin[1], Qiong Yi[2], Jiali Guo[1], and Feng Xiao[1,*]

[1]Department of Anesthesiology, the Second Xiangya Hospital, Central South University, Changsha 410011, China, and [2]Department of Intensive Care Unit, the First Hospital of Hunan University of Chinese Medicine, Hunan University of Chinese Medicine, Changsha 410007, China
*Correspondence address: Tel: +86-13607430840; E-mail: xiaofengcsu@csu.edu.cn

Received 29 November 2023 Accepted 27 December 2023

Abstract

Myocardial damage is a critical complication and a significant contributor to mortality in sepsis. MicroRNAs (miRNAs) have emerged as key players in sepsis pathogenesis. In this study, we explore the effect and mechanisms of miR-29b-1-5p on sepsis-induced myocardial damage. Sepsis-associated Gene Expression Omnibus datasets (GSE72380 and GSE29914) are examined for differential miRNAs. The mouse sepsis-induced cardiac injury was established by Lipopolysaccharide (LPS) or cecal ligation and puncture (CLP). LPS-treated HL-1 mouse cardiomyocytes simulate myocardial injury *in vitro*. miR-29b-1-5p is co-upregulated in both datasets and in cardiac tissue from sepsis mouse and HL-1 cell models. miR-29b-1-5p expression downregulation was achieved by antagomir transduction and confirmed by real-time quantitative reverse transcription PCR. Survival analysis and echocardiography examination show that miR-29b-1-5p inhibition improves mice survival cardiac function in LPS- and CLP-induced sepsis mice. Hematoxylin and eosin and Masson's trichrome staining and Immunohistochemistry analysis of mouse myocardial α-smooth muscle actin show that miR-29b-1-5p inhibition reduces myocardial tissue injury and fibrosis. The inflammatory cytokines and cardiac troponin I (cTnI) levels in mouse serum and HL-1 cells are also decreased by miR-29b-1-5p inhibition, as revealed by enzyme-linked immunosorbent assay. The expressions of autophagy-lysosomal pathway-related and apoptosis-related proteins in the mouse cardiac tissues and HL-1 cells are evaluated by western blot analysis. The sepsis-induced activation of the autophagy-lysosomal pathway and apoptosis are also reversed by miR-29b-1-5p antagomir. MTT and flow cytometry measurement further confirm the protective role of miR-29b-1-5p antagomir in HL-1 cells by increasing cell viability and suppressing cell apoptosis. Metascape functionally enriches TargetScan-predicted miR-29b-1-5p target genes. TargetScan prediction and dual luciferase assay validate the targeting relationship between miR-29b-1-5p and telomeric repeat-binding factor 2 (TERF2). The expression and function of TERF2 in HL-1 cells and mice are also evaluated. MiR-29b-1-5p negatively regulates the target gene *TERF2*. *TERF2* knockdown partly restores miR-29b-1-5p antagomir function in LPS-stimulated HL-1 cells. In summary, miR-29b-1-5p targetedly inhibits TERF2, thereby enhancing sepsis-induced myocardial injury.

Key words sepsis, myocardial injury, miR-29b-1-5p, telomeric repeat-binding factor 2 (TERF2), apoptosis, autophagy

Introduction

Sepsis is defined as a potentially fatal multiorgan failure resulted from a deficient response of a host to a serious infection [1,2]. Sepsis is one of the leading causes of morbidity and mortality worldwide due to the lack of effective interventions [3]. Sepsis-induced cardiomyopathy is a common myocardial dysfunction induced by sepsis, the pathophysiologic process of which is reversible [4]. Research indicated that patients suffering from both sepsis and myocardial dysfunction are at a mortality risk of 70%–90%, superseding the risk faced by patients who have no myocardial damage (20%) [3,4]. Effective therapies are still unavailable despite the exploration of multiple approaches to prevent sepsis-induced

myocardial dysfunction [5,6]. Therefore, there is a pressing need to identify new treatments to decrease the morbidity and mortality rate of septic patients.

MicroRNAs (miRNAs) are single-stranded noncoding RNAs containing ~22 nucleotides that are highly conserved in different species. miRNAs can target the 3′ untranslated region (3′UTR) of mRNAs to exert a negative regulatory effect on gene expression, thereby resulting in the repression or decay of mRNA targets [7]. Reportedly, miRNAs might participate in nearly all key cellular functions, such as growth, differentiation, proliferation, and apoptosis [8]. As previously reported, miRNAs are linked to multiple disorders, such as sepsis, heart disease, and diabetes [9–11]. According to recent studies, miRNAs have a significant impact on the development of cardiac damage during sepsis [12,13]. Therefore, investigating the specific function of miRNAs in myocardial dysfunction in sepsis and their underlying mechanisms may contribute to the development of novel, efficacious therapeutic approaches for individuals suffering from myocardial injury in sepsis.

Bioinformatics data mining through gene and noncoding RNA microarray data is useful for identifying novel important genes and noncoding RNAs related to disease pathogenesis [14]. Microarrays have been used to screen for differential miRNAs and mRNAs involved in diseases such as cancer [15], sepsis, and acute kidney injury [16]. Previous studies have also reported differentially expressed genes (DEGs) in patients with septic myocardial injury via microarray microarrays [17]. Therefore, it is feasible to investigate the molecular pathways involved in septic myocardial injury via the use of microarrays.

In this study, miR-29b-1-5p, a differentially expressed miRNA, was obtained through Gene Expression Omnibus (GEO) microarray and bioinformatics screening. *In vivo* and *in vitro* models revealed that inhibition of miR-29b-1-5p ameliorated septic myocardial injury-related cardiomyocyte dysfunction, and this effect was achieved by upregulation of telomeric repeat-binding factor 2 (TERF2).

Materials and Methods

Septic myocardial injury animal model

Male C57BL/6 mice weighing 23 ± 2 g and 8 weeks old were procured from Hunan SJA Laboratory Animal Co. (Changsha, China), and housed in a specific pathogen-free (SPF) environment with a temperature range of 23–25°C and a humidity level of 55% ± 5%. The mice were allowed free access to a standard chow diet and drinking water. The experimental procedures included in this study involving animals were approved by the Ethics Committee of Second Xiangya Hospital (approval No: 2021347).

An LPS-induced sepsis mouse model was established as previously reported [18]. Mice were anaesthetized by inhalation with 3% isoflurane and then intraperitoneally injected with 10 mg/kg LPS (from *055:B5*, L8880; Solarbio, Beijing, China). An equal amount of saline was injected into the control group. The cecal ligation and puncture (CLP) sepsis models were established in mice as follows. Mice were anaesthetized with isoflurane. A 1–2 cm abdominal midline incision was made to expose the cecum. After ligating the distal part of the cecum, the ligated segment was punctured once with a 22G needle. The appendix was repositioned and injected subcutaneously with 1 mL of sterile saline. The incision was closed with a 9-mm steel wound clip. miR-29b-1-5p was downregulated or overexpressed by tail vein injection of 80 mg/kg mmu-miR-29b-1-5p antagomir or 30 mg/kg agomir (General Biol, Chuzhou, China) dissolved in 100 μL of sterile saline daily for 3 days [19–21] prior to LPS injection or CLP surgery. Echocardiographic testing was performed 24 h after LPS induction or CLP surgery. After echocardiographic testing, the mice were euthanized by intraperitoneal injection of pentobarbitone (200 mg/kg) immediately, after which heart tissue and blood sample were harvested. Six mice were used per group. The sequences of agomir and antagomir are listed in Table 1.

For survival analysis, 20 additional mice were taken from each group according to previous methods [22]. The mouse model of LPS-induced sepsis was induced using the aforementioned procedure, and the LPS dose was adjusted to 25 mg/kg [23] to achieve a lethal dose. The CLP model was generated using the same procedure as described above. Mice were observed for survival every 24 h for 96 h.

Echocardiography

Mice were anaesthesized via inhalation of isoflurane and a heating pad was used to maintain their core temperature at the same level 24 h after LPS induction or CLP surgery. A VisualSonics Vevo-3100 Ultrasound (FUJIFILM VisualSonics, Tokyo, Japan) was used for echocardiography measurements. The Vevo 3100 imaging program was used to analyze the M-mode images taken along the short axis of the left ventricle. Left ventricle end-systolic diameters (LVIDs) and left ventricle end-diastolic diameters (LVIDd) were used to calculate fractional shortening (FS): FS (%) = [(LVIDd–LVIDs)/LVIDd] × 100%; and both the end-diastolic and end-systolic volumes of the left ventricle (EDV and ESV, respectively) were assessed to calculate the ejection fraction (EF): EF (%) = [(EDV–ESV)/EDV] × 100% [24].

Histological testing

After being fixed in 4% formaldehyde, the heart tissues were cut transversely into paraffin-embedded sections (4-μm sections). The tissue sections were dewaxed using xylene (Beyotime, Shanghai, China) and rehydrated using gradient alcohol. Histological staining was performed using a haematoxylin and eosin (H&E) staining kit and a Masson's staining kit (Solarbio, Beijing, China), followed by dehydration and transparency [25,26]. Neutral resin was used to seal the slices, which were observed under a light microscope (Tokyo, Japan). The cardiac injury score was measured based on HE staining as previously described [27]. Briefly, 0 = no lesion, 1 = myocardial damage < 25%, 2 = myocardial damage 25%–50%, 3 = myocardial damage 50%–75%, and 4 = myocardial damage > 75%. The fibrotic area was measured based on Masson's trichrome staining using ImageJ software (NIH, Bethesda, USA).

Table 1. The sequences of agomir and antagomir

Name	Sequence (5′→3′)	
miR-29b-1-5p agomir	Sense	GCUGGUUUCAUAUGGUGGUUUA
	Antisense	AACCACCAUAUGAAACCAGCUU
NC agomir	Sense	UUCUCCGAACGUGUCACGUTT
	Antisense	ACGUGACACGUUCGGAGAATT
miR-29b-1-5p antagomir	UAAACCACCAUAUGAAACCAGC	
NC antagomir	CAGUACUUUUGUGUAGUACAA	

The sections were assessed by pathologists through a double-blind analysis under an optical microscope (Olympus).

Immunohistochemical (IHC) staining

After being routinely dewaxed and rehydrated, the slices were heated thrice for 5 min each in pH 6.0 antigen repair solution and washed with PBS. Then, 3% hydrogen peroxide solution was added to the slices (Beyotime), which were incubated for 25 min, washed with PBS, and blocked with 3% bovine serum albumin (BSA; Servicebio, Wuhan, China) for 30 min at room temperature (RT). The slices were rinsed, followed by overnight incubation at 4°C with anti-α-SMA (1:50; ab5694; Abcam, Cambrige, UK) and then a 50-min incubation at room temperature with horseradish peroxidase (HRP)-coupled anti-IgG (1:50; ab270144; Abcam). A 3,3′-diaminobenzidine (DAB) color development solution (Servicebio) was used to develop slices for 3 min. Tap water was subsequently used to rinse the slices. The sections were restained with hematoxylin for an additional 3 min after being cleaned with tap water. Sections were dehydrated using gradient ethanol, sealed with xylene transparently, and finally observed under a light microscope [28,29]. α-SMA protein expression is shown in brown. The optical density of the α-SMA signal was assessed by ImageJ software (NIH).

Cell processing and transfection

The HL-1 mouse cardiomyocyte cell line was procured from Procell (Wuhan, China). The cells were subsequently cultured in Dulbecco's modified Eagle's medium (DMEM) supplemented with 10% foetal bovine serum (FBS) at 37°C in a 5% CO_2 atmosphere. After 24 h, HL-1 cells were exposed to 1 μg/mL LPS [30]. HL-1 cells was transfected with the miR-29b-1-5p antagomir (General Biol) at a final concentration of 50 nM, or the NC antagomir (negative control; General Biol), the TERF2 shRNA vector (GenePharma, Shanghai, China) at a final concentration of 1 μg/mL, or the sh-NC vector (negative control; GenePharma) using Lipofectamine 2000 (Thermo Fisher Scientific, Waltham, USA). The transduction of cells was performed 24 h before LPS induction. The sequences for vector construction are listed in Table 2.

Enzyme-linked immunosorbent assay (ELISA)

Mouse serum or HL-1 cell supernatant was collected. The levels of tumor necrosis factor α (TNF-α), interleukin (IL)-1β, IL-6, and cardiac troponin I (cTnI) were measured separately using the corresponding ELISA kits according to the manufacturer's instructions. The kits included TNF-α (SEKM-0034; Solarbio), mouse IL-6 (SEKM-0007; Solarbio), IL-1β (SEKM-0002; Solarbio), and mouse cTnI (KS11280; Keshun Science and Technology, Shanghai, China).

qRT-PCR

TRIzol was used to extract total RNA from mouse left ventricle tissue and HL-1 cells. A spectrophotometer was used to measure the RNA concentration and quality. A TaqMan microRNA reverse transcription kit (Applied Biosystems, Waltham, USA) was used for miRNA reverse transcription. A reverse transcription kit (Genecopoeia, Guangzhou, China) was used for reverse transcription of the mRNA to cDNA. SYBR Premix Ex Taq (Takara, Dalian, China) was used on an ABI 7500HT system (Applied Biosystems) for quantitative real-time PCR. The $2^{-\Delta\Delta Ct}$ method [31] was used for data processing and analysis. *U6* was used as the miRNA internal control, while *GAPDH* was used as the internal reference for mRNA expression. Table 3 lists the sequences of the primers.

Western blot analysis

RIPA lysis buffer (Beyotime) was used to extract total protein from HL-1 cells or mouse left ventricle tissues, and the total protein concentration was determined using a BCA kit (Beyotime) as previously described [32]. After separation by 10% sodium dodecyl sulfate-polyacrylamide gel electrophoresis (SDS-PAGE), 50 μg of total protein was transferred to PVDF membranes (Millipore, Billerica, USA), which were blocked with 5% skim milk in TBST solution for 2 h. Then the membranes were incubated overnight at

Table 2. The sequences of sh-NC vector and sh-TERF2

Name	Sequence (5′→3′)	
sh-NC	Sense	GATCCGCAGATGAAGGCACGGTCACGCTCGAGCGTGACCGTGCCTTCATCTGCTTTTTG
	Antisense	AATTCAAAAAGCAGATGAAGGCACGGTCACGCTCGAGCGTGACCGTGCCTTCATCTGCG
Sh-TERF2	Sense	GATCCGGCTTTCAAAGCTCTGTCTACTCTCGAGAGTAGACAGAGCTTTGAAAGCTTTTTG
	Antisense	AATTCAAAAAGCTTTCAAAGCTCTGTCTACTCTCGAGAGTAGACAGAGCTTTGAAAGCG

Table 3. The sequences of the primers used in this study

Gene	Sequence (5′→3′)	
miR-29b-1-5p	RT primer	GTCGTATCCAGTGCGTGTCGTGGAGTCGGCAATTGCACTGGATACGACTAAACC
	Forward primer	GCGCTGGTTTCATATGGT
	Reverse primer	CAGTGCGTGTCGTGGA
U6	Forward primer	CTCGCTTCGGCAGCACA
	Reverse primer	AACGCTTCACGAATTTGCGT
TERF2	Forward primer	CTGTCTACTGCACAAGACTCAG
	Reverse primer	TGCCAGATTAGCAAGTACCAGA
GAPDH	Forward primer	AGGTCGGTGTGAACGGATTTG
	Reverse primer	TGTAGACCATGTAGTTGAGGTCA

RT: reverser transcription.

4°C with the following antibodies: anti-TERF2 (1:1000; 66893-1-Ig; Proteintech, Wuhan, China), anti-Bax (1:1000; ab32503; Abcam), anti-Bcl-2 (1:2000; ab182858; Abcam), anti-cleaved caspase-3 (1:5000; ab214430; Abcam), anti-Pro-caspase-3 (1:10,000; ab32499; Abcam), anti-cleaved PARP (1:1000; ab32064; Abcam), anti-TLR2 (1:1000; DF7002; Affinity Bioscience, Beijing, China), anti-TLR4 (1:1000; 19811-1-AP; Proteintech), anti-TFEB (1:1000; 13372-1-AP; Proteintech), anti-LAMP1(1:1000; 67300-1-Ig; Proteintech), anti-LC3II (1:1000; 14600-1-AP; Proteintech), anti-β-actin (1:1000; ab8227; Abcam), and anti-GAPDH (1:1000, AF7021; Affinity Bioscience), followed by incubation with HPR-conjugated goat anti-mouse or rabbit IgG secondary antibody (1:2000; SA00001-2 or SA00001-1; Proteintech) for 2 h at room temperature. Finally, protein bands were visualized using an enhanced chemiluminescence (ECL) kit (Xinsamax, Suzhou, China). β-Actin or GAPDH was used as the internal control.

MTT assay

HL-1 cells from different groups were inoculated at a density of 5×10^3 cells/well in 96-well plates and cultured for 0, 24, 48, or 72 h. At each time point, MTT solution (50 μL; Beyotime) was added to each well in each group and incubated for 4 h at 37°C. After the MTT and culture medium mixture were discarded, 150 μL dimethyl sulfoxide was added to each well to dissolve the crystals, and the absorbance was measured at 490 nm using a multifunctional microplate reader (PerkinElmer, Waltham, USA).

Flow cytometry analysis of cell apoptosis

As per the manufacturer's instructions, an Annexin V-FITC/PI Apoptosis Detection kit (Keygene, Nanjing, China) was used to assess apoptosis. After treatment, the cells were collected and resuspended in 500 μL of binding buffer. The suspension was subsequently stained with PI staining solution and Annexin V-FITC staining solution, each in a volume of 5 μL, at room temperature for 5–10 min in the dark. NovoCyte Flow cytometry (Agilent, Santa Clara, USA) analysis was conducted immediately after collection.

Bioinformatics analysis

The GSE72380, GSE29914, and GSE185754 datasets were downloaded from the GEO database (https://www.ncbi.nlm.nih.gov/geo/) for analysis of differentially expressed miRNAs and mRNAs in dysfunctional septic cardiac tissues from mice. The mmu-miR-29b-1-5p-targeted genes were predicted by TargetScan (https://www.targetscan.org/vert_72/) with a threshold of total context + + score ≤–0.3. The functional enrichment of the mmu-miR-29b-1-5p downstream target gene set was analyzed via Metascape (https://metascape.org/gp/index.html#/main/step1).

Dual-luciferase reporter gene assay

The use of TargetScan allowed the prediction of potential binding sites between miR-29b-1-5p and TERF2. The miR-29b-1-5p binding site was introduced into the TERF2 3′UTR wild-type (WT) and TERF2 3′UTR mutant (MUT) sequences before being inserted into the psi-CHECK2 luciferase vector to create the psi-CHECK2-TERF2-WT and psi-CHECK2-TERF2-MUT vectors. HL-1 cells were cotransfected with the aforementioned vectors and miR-29b-1-5p agomir or NC agomir using Lipofectamine 2000. Forty-eight hours after transfection, the relative luciferase activity was measured using a dual luciferase reporter kit (Promega, Madison, USA) as directed by the manufacturer.

Statistical analysis

The results were analyzed using GraphPad Prism 8.0 (GraphPad Software, La Jolla, USA). Data are presented as the mean ± the standard deviation (SD). One-way ANOVA with Tukey post hoc test was carried out to analyze the differences among more than two groups. Student's *t* test was carried out to analyze the difference between two groups. Pearson's correlation analysis was also conducted. A *P* value of less than 0.05 was considered statistically significant.

Results

GEO dataset screening for septic myocardial injury-associated miRNAs

Differentially expressed miRNAs in normal cardiac tissues and septic cardiac tissues from mice were analyzed from the GSE72380 and GSE29914 microarray datasets. Three significantly downregulated miRNAs and 8 significantly upregulated miRNAs (Figure 1A,B; $|\log_2 FC| > 0.4$, $P < 0.05$) were obtained from the GSE72380 microarray. Three differentially upregulated miRNAs and 1 differentially downregulated miRNA were obtained from the GSE29914 chip (Figure 1C,D; $|\log_2 FC| > 0.4$, $P < 0.05$). Two codifferentially expressed miRNAs, *i.e.*, miR-29b-1-5p and miR-155, were obtained (Figure 1E). The role of miR-155 in sepsis has been reported [33,34]. Therefore, miR-29b-1-5p was chosen for further investigation. It was upregulated in both the GSE72380 and GSE29914 (Figure 1F–G).

Inhibition of miR-29b-1-5p ameliorates LPS-induced septic myocardial injury in mice

The function of miR-29b-1-5p was subsequently explored in a mouse sepsis model. A mouse model of septic myocardial injury was induced by LPS. The survival rate of the mice after LPS treatment was lower than that of the control group (Figure 2A), and the EF and FS were significantly reduced (Figure 2B). However, LVIDd (mm), LVIDs (mm), and heart rate were significantly greater in LPS-treated mice than in control mice (Table 4). H&E and Masson's trichrome staining revealed that mice in the control group had clear myocardial fibers and uniform and clear myocardial cell spacing without degeneration or necrosis, while the myocardial cells in the LPS-treated mice were significantly fractured and deformed and had lysed myocardial fibers with enhanced fibrosis (Figure 2C,D). Correspondingly, the cardiomyocyte injury score and fibrotic area were increased in LPS-treated mice (Figure 2F,G). IHC staining revealed that α-SMA level in the myocardial tissues of LPS-treated mice was significantly increased (Figure 2E,H). ELISA results for inflammatory cytokines showed that TNF-α, IL-1β, and IL-6 levels in mouse serum were markedly increased (Figure 2I–K), and in addition, the expression level of cTnI in mouse serum was also significantly increased (Figure 2L). qRT-PCR revealed that LPS promoted miR-29b-1-5p expression in the myocardial tissues of the mice (Figure 2M). Accumulating evidence indicates that the autophagy-lysosomal pathway, which plays a fundamental role in cellular homeostasis and antimicrobial immunity, is commonly impaired in sepsis [35]. Therefore, changes in the expressions of autophagy-lysosomal pathway-related proteins were also determined. As shown in Figure 2N, the expressions of TLR2, TLR4,

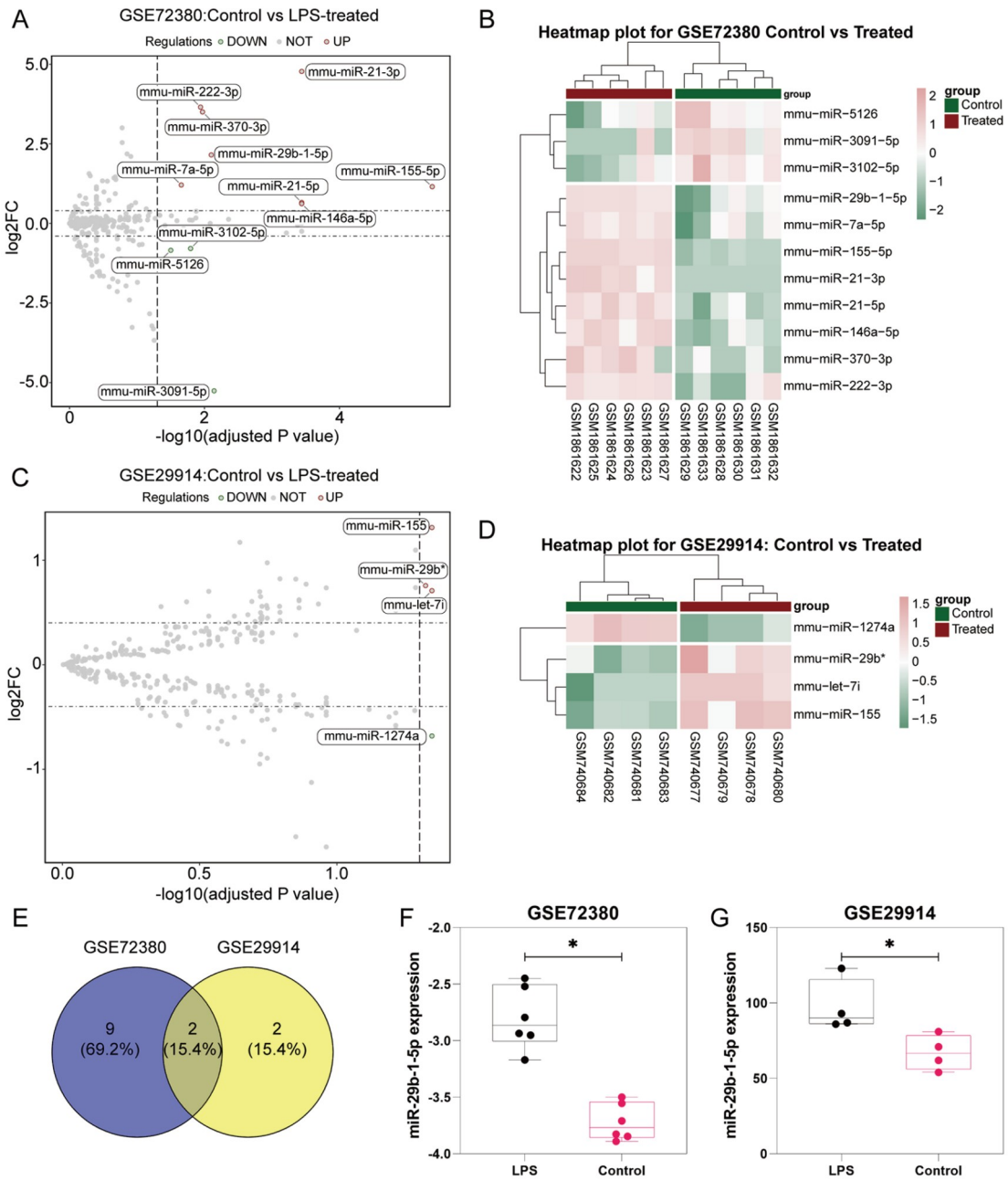

Figure 1. Gene Expression Omnibus (GEO) dataset screening for septic myocardial injury-associated miRNAs (A) Volcano plot and (B) heatmap of GSE72380. (C) Volcano plot and (D) heatmap of GSE29914. (E) Venn diagram of the differentially expressed genes identified in the GSE72380 and GSE29914 cohorts according to the intersection ($|\log_2 FC| > 0.4$, $P < 0.05$). (F,G) Expression of miR-29b-1-5p in the GSE72380 and GSE29914 cohorts. $^*P < 0.05$.

TFEB, LAMP1, and LC3II increased in LPS-treated mice, indicating that LPS treatment activated the lysosomal pathway in the cardiac tissues of model mice. miR-29b-1-5p expression in the myocardial tissue of mice was subsequently inhibited by miR-29b-1-5p antagomir injection (Figure 2M). The inhibition of miR-29b-1-5p promoted survival; increased EF and FS; decreased LVIDd (mm), LVIDs (mm), and heart rate; alleviated the degree of myocardial tissue injury and fibrosis in mice; and significantly decreased the α-SMA, TNF-α, IL-1β, L-6 and cTnI levels (Figure 2A–L and Table 4). In contrast, the miR-29b-1-5p agomir further increased LPS-induced septic myocardial injury and inflammation (Supplementary Figure S1). Interestingly, the miR-29b-1p antagomir inhibited LPS-induced activation of the lysosomal pathway by reducing the expressions of TLR2, TLR4, TFEB, LAMP1, and LC3II (Figure 2N). These findings imply that miR-29b-1-5p silencing can mitigate LPS-induced septic myocardial damage in mice.

Inhibition of miR-29b-1-5p ameliorates CLP-induced septic myocardial injury in mice

The CLP model is currently the gold standard for sepsis studies [36]. Thus, to further validate the role of miR-29b-1-5p, a mouse model of CLP-induced septic myocardial injury was used. The results showed

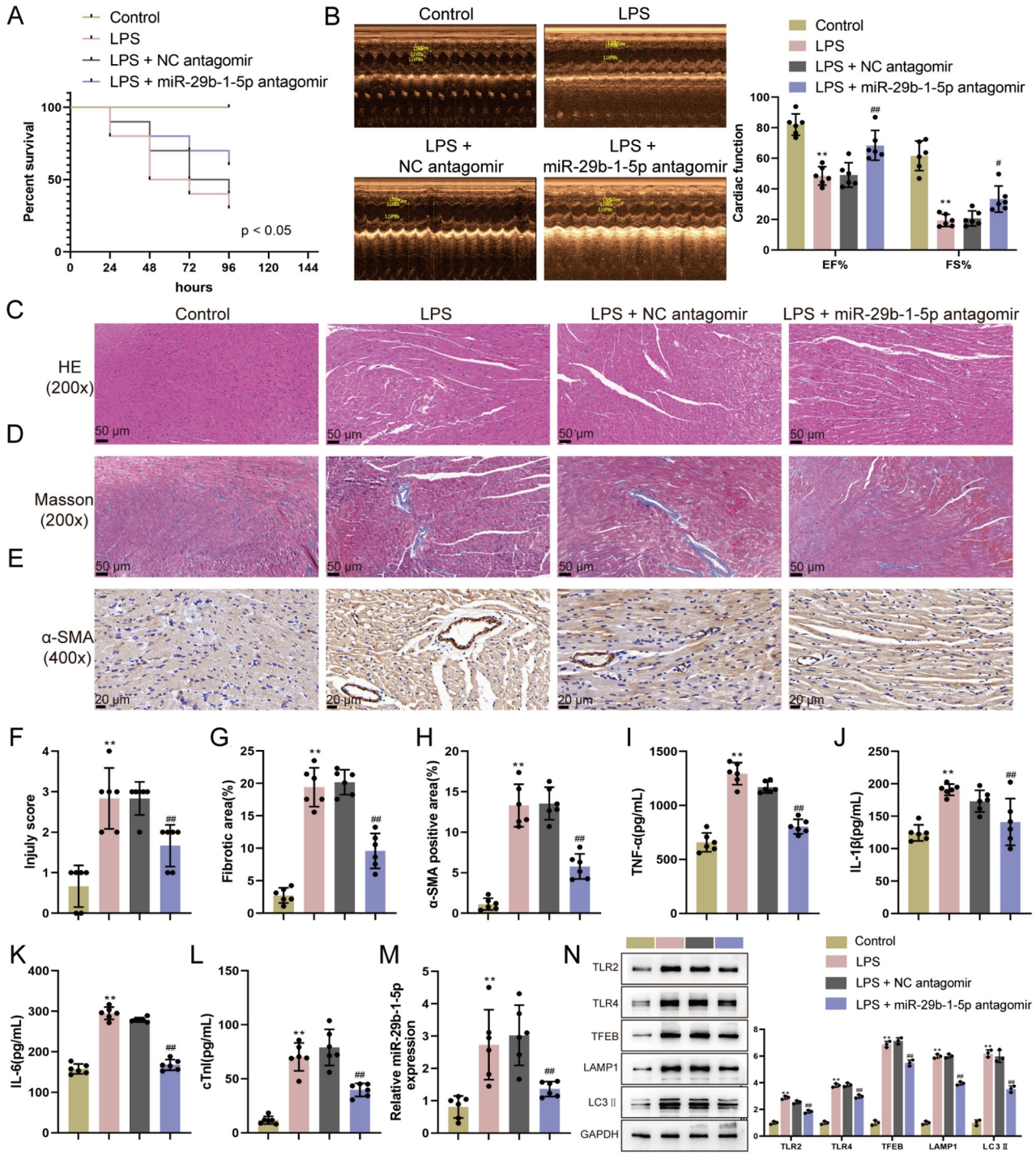

Figure 2. Inhibition of miR-29b-1-5p ameliorates lipopolysaccharide (LPS)-induced septic myocardial injury in mice (A) Mice received a single intraperitoneal injection of 25 mg/kg LPS (lethal dose) or a tail vein injection of 80 mg/kg miR-29b-1-5p/NC antagomir for 3 consecutive days (24 h later receiving LPS injection), after which the survival conditions were assessed for 96 h, and survival rate curves were generated. An equal amount of saline was injected into the control group. $n = 20$. Mice received a single intraperitoneal injection of 10 mg/kg LPS or a tail vein injection of 80 mg/kg miR-29b-1-5p/NC antagomir for 3 consecutive days (24 h later receiving LPS injection). (B) Twenty-four hours after LPS injection, echocardiography tests were performed. (C,D) Mice were euthanized, and histological analysis of myocardial tissue injury was performed via hematoxylin and eosin (HE) staining and Masson's trichrome staining. Scale bar: 50 μm. (F,G) The cardiac injury score and fibrotic area were assessed via HE and Masson's trichrome staining, respectively. (E,H) α-Smooth muscle actin (α-SMA) expression in mouse myocardial tissues was determined via immunohistochemistry (IHC) staining. Scale bar: 20 μm. (I–L) Tumor necrosis factor-α (TNF-α), interleukin (IL)-1β, IL-6 and cardiac troponin I (cTnI) levels in mouse serum were determined by enzyme-linked immunosorbent assay (ELISA). (M) The miR-29b-1-5p expression level in mouse myocardial tissue was determined by real-time quantitative reverse transcription PCR (qRT-PCR). $n = 6$. (N) The protein levels of TLR2, TLR4, TFEB, LAMP1 and LC3II in mouse myocardial tissues were determined by western blot analysis. $n = 3$. $^{**}P < 0.01$ vs the control group; $^{\#}P < 0.05$ and $^{\#\#}P < 0.01$ vs. the LPS + NC antagomir group.

Table 4. Echocardiography data of LPS-induced sepsis model

Parameter	Control	LPS	LPS + NC antagomir	LPS + miR-29b-1-5p antagomir
Ejection fraction (%)	82.04 ± 7.00	48.55 ± 6.02**	49.13 ± 8.10	68.49 ± 9.80##
Fractional shortening (%)	61.64 ± 9.70	19.42 ± 3.99**	20.72 ± 5.33	33.37 ± 8.55#
LVIDd (mm)	1.78 ± 0.10	2.39 ± 0.11**	2.45 ± 0.11	1.81 ± 0.20##
LVIDs (mm)	0.68 ± 0.15	1.92 ± 0.13**	1.94 ± 0.10	1.16 ± 0.25##
Heart rate (bpm)	471.67 ± 56.83	541.83 ± 49.22*	534.17 ± 23.38	464.00 ± 19.37#

*$P < 0.05$, **$P < 0.01$ vs control group; #$P < 0.05$, ##$P < 0.01$ vs LPS+NC antagomir.

that mice in the CLP group had reduced survival rate, reduced EF and FS (Figure 3A,B), increased LVIDd (mm), LVIDs (mm), and heart rate (Table 5), apparent myocardial tissue injury and enhanced fibrosis, and elevated α-SMA expression in the myocardium compared with those in the control group (Figure 3C–H). The expressions of TNF-α, IL-1β, L-6, and cTnI in the serum were increased, and the expression of miR-29b-1-5p was upregulated in myocardial tissues (Figure 3I–M). Moreover, the expressions of TLR2, TLR4, TFEB, LAMP1, and LC3II were also increased in CLP mice (Figure 3N). These CLP-induced changes could be reversed by the inhibition of miR-29b-1-5p (Figure 3A–N). Conversely, the miR-29b-1-5p agomir further increased CLP-induced septic myocardial injury and inflammation (Supplementary Figure S2). The above findings suggest that miR-29b-1-5p suppression protects mice from CLP-induced septic myocardial injury.

Inhibition of miR-29b-1-5p ameliorates LPS-induced cardiomyocyte dysfunction *in vitro*

The functional role of miR-29b-1-5p in cardiomyocyte dysfunction in mice was further explored in a cellular model. A septic myocardial injury cell model was induced by LPS in HL-1 cells. HL-1 cells were treated with the miR-29b-1-5p antagomir, and qRT–PCR was subsequently used to analyze the extent of the inhibition. Compared to the control group, the LPS-induced HL-1 cells exhibited upregulation of miR-29b-1-5p. However, after transduction with the miR-29b-1-5p antagomir, this upregulation was considerably reduced (Figure 4A). Moreover, LPS treatment inhibited HL-1 cell viability, which was significantly increased following the inhibition of miR-29b-1-5p (Figure 4B). Flow cytometry assays showed that HL-1 cell apoptosis was induced by LPS, which was inhibited by miR-29b-1-5p antagomir transfection (Figure 4C). According to the ELISA results, TNF-α, IL-1β, and IL-6 levels were considerably greater in the cells of the LPS group than in cells of the control group. However, these levels were lower after miR-29b-1-5p antagomir transduction (Figure 4D–F). Concerning apoptotic markers, LPS stimulation increased the levels of the proapoptotic proteins Bax and cleaved caspase-3 while decreasing the level of the antiapoptotic protein Bcl-2. Inhibition of miR-29b-1-5p increased Bcl-2 level while simultaneously decreasing Bax and cleaved caspase-3 levels (Figure 4G–H). Consistent with the *in vivo* results, LPS-induced upregulation of TLR2, TLR4, TFEB, LAMP1, and LC3II was also reduced by inhibition of miR-29b-1-5p (Figure 4I). Therefore, miR-29b-1-5p inhibition can ameliorate LPS-induced cardiomyocyte dysfunction in mice *in vitro*.

TERF2 is a downstream target of miR-29b-1-5p

Additional screening for downstream targets of miR-29b-1-5p was carried out, and the results showed that the TargetScan online database predicted 214 target genes. The target genes were then functionally enriched by Metascape and were found to be associated with the cell cycle pathway (Figure 5A,B). The GSE185754 microarray analysis of target genes associated with cell cycle pathways revealed that EP300, TERF2, MLH3, and POLD4 expressions were significantly downregulated in patients with sepsis (Figure 5C). Validation by qRT-PCR in LPS-treated HL-1 cells indicated that these 4 factors were downregulated in the LPS group of cells, with the most significant difference in TERF2 expression (Supplementary Figure S3A–D). Therefore, TERF2 was selected for subsequent analyses. Consistent with our prediction, miR-29b-1-5p was able to bind to the *TERF2* 3′UTR (Figure 5D). LPS treatment downregulated TERF2 mRNA and protein expression, while the miR-29b-1-5p antagomir upregulated TERF2 mRNA and protein expression (Figure 5E,F). The correlation between TERF2 mRNA and miR-29b-1-5p levels in mouse cardiac tissues was determined. The expressions of TERF2 and miR-29b-1-5p were negatively correlated in the cardiac tissue of mice in the LPS and CLP mouse models. (Figure 5G).

Silencing of *TERF2* partially reverses the protective effect of miR-29b-1-5p inhibition on LPS-induced cardiomyocyte apoptosis and inflammation

The role of TERF2 in myocardial functional impairment in sepsis was further explored *in vitro*. In HL-1 cells, the introduction of the shTERF2 vector resulted in the inhibition of TERF2 expression, and the efficacy of the transfection was assessed by immunoblotting (Figure 6A). After LPS treatment, silencing of *TERF2* impacted HL-1 cell viability; promoted apoptosis; increased TNF-α, IL-1β and IL-6 levels; increased cleaved PARP, cleaved caspase-3, TLR2, TLR4, TFEB, LAMP1 and LC3II levels; and partially abolished the protective effect of the miR-29b-1-5p antagomir on HL-1 cell function (Figure 6B–I). The above results indicate that silencing of *TERF2* can partially reverse the protective effects of miR-29b-1-5p inhibition on LPS-induced cardiomyocyte apoptosis and the inflammatory response.

Discussion

Myocardial damage is one of the most serious consequences of sepsis and is the major cause of mortality in critical care units [37]. miRNAs have been reported to participate in sepsis-induced myocardial injury and serve as diagnostic markers and/or treatment targets [38]. Here, bioinformatics analysis of the sepsis-associated datasets GSE72380 and GSE29914 identified that miR-29b-1-5p is upregulated in both datasets. A previous study reported that miR-29b-1-5p caused apoptosis in ischaemia–reperfusion–induced myocardial injury [39]; however, the role of miR-29b-1-5p has not been reported in sepsis-induced myocardial injury. Therefore, it is hypothesized that miR-29b-1-5p has a potential mechanism of action in septic myocardial injury.

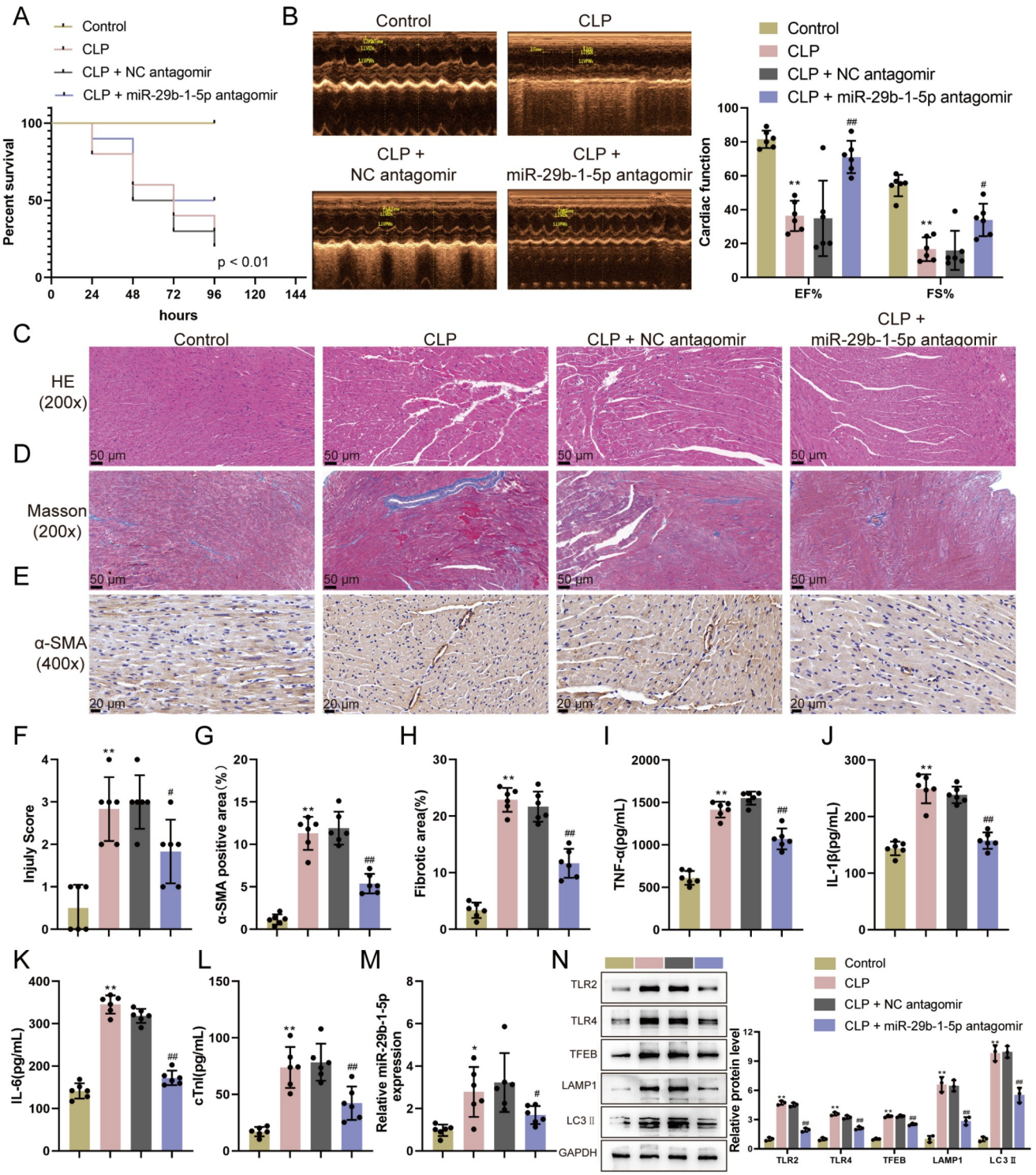

Figure 3. Inhibition of miR-29b-1-5p ameliorates CLP-induced septic myocardial injury in mice (A) Mice were subjected to CLP surgery or tail vein injection of 80 mg/kg miR-29b-1-5p/NC antagomir for 3 consecutive days (24 h later receiving CLP surgery), after which the survival conditions were assessed for 96 h, and survival rate curves were generated. $n = 20$. A sham operation was performed on the control group. $n = 20$. (B) Twenty-four hours after CLP surgery, echocardiography was performed. (C,D) Mice were euthanized, and histological analysis of myocardial tissue injury was performed via HE staining and Masson's trichrome staining. Scale bar: 50 μm. (F,G) The cardiac injury score and fibrotic area were assessed via HE and Masson's trichrome staining, respectively. (E,H) The protein levels and distribution of α-SMA in mouse myocardial tissues were examined using IHC staining. Scale bar: 20 μm. (I–L) TNF-α, IL-1β, IL-6 and cTnI levels in mouse serum were determined by ELISA. (M) The miR-29b-1-5p expression level in mouse myocardial tissue was determined by qRT-PCR. $n = 6$. (N) The protein levels of TLR2, TLR4, TFEB, LAMP1 and LC3II in mouse myocardial tissues were determined by western blot analysis. $n = 3$. $^{**}P < 0.01$ vs the control group; $^{\#}P < 0.05$ and $^{\#\#}P < 0.01$ vs the CLP + NC antagomir group.

Table 5. Echocardiography data of CLP-induced sepsis model

Parameter	Control	CLP	CLP + NC antagomir	CLP + miR-29b-1-5p antagomir
Ejection fraction (%)	81.53 ± 5.13	36.35 ± 8.93**	34.89 ± 21.49	71.07 ± 9.53##
Fractional shortening (%)	54.30 ± 6.30	16.70 ± 7.00**	15.98 ± 11.67	33.95 ± 9.56#
LVIDd (mm)	1.79 ± 0.09	2.49 ± 0.25**	2.51 ± 0.20	2.14 ± 0.29#
LVIDs (mm)	0.82 ± 0.13	2.07 ± 0.24**	2.11 ± 0.32	1.42 ± 0.14##
Heart rate (bpm)	457.67 ± 29.80	534.00 ± 23.15**	533.33 ± 34.09	480.00 ± 35.41#

*$P < 0.05$, **$P < 0.01$ vs control group; #$P < 0.05$, ##$P < 0.01$ vs CLP+NC antagomir.

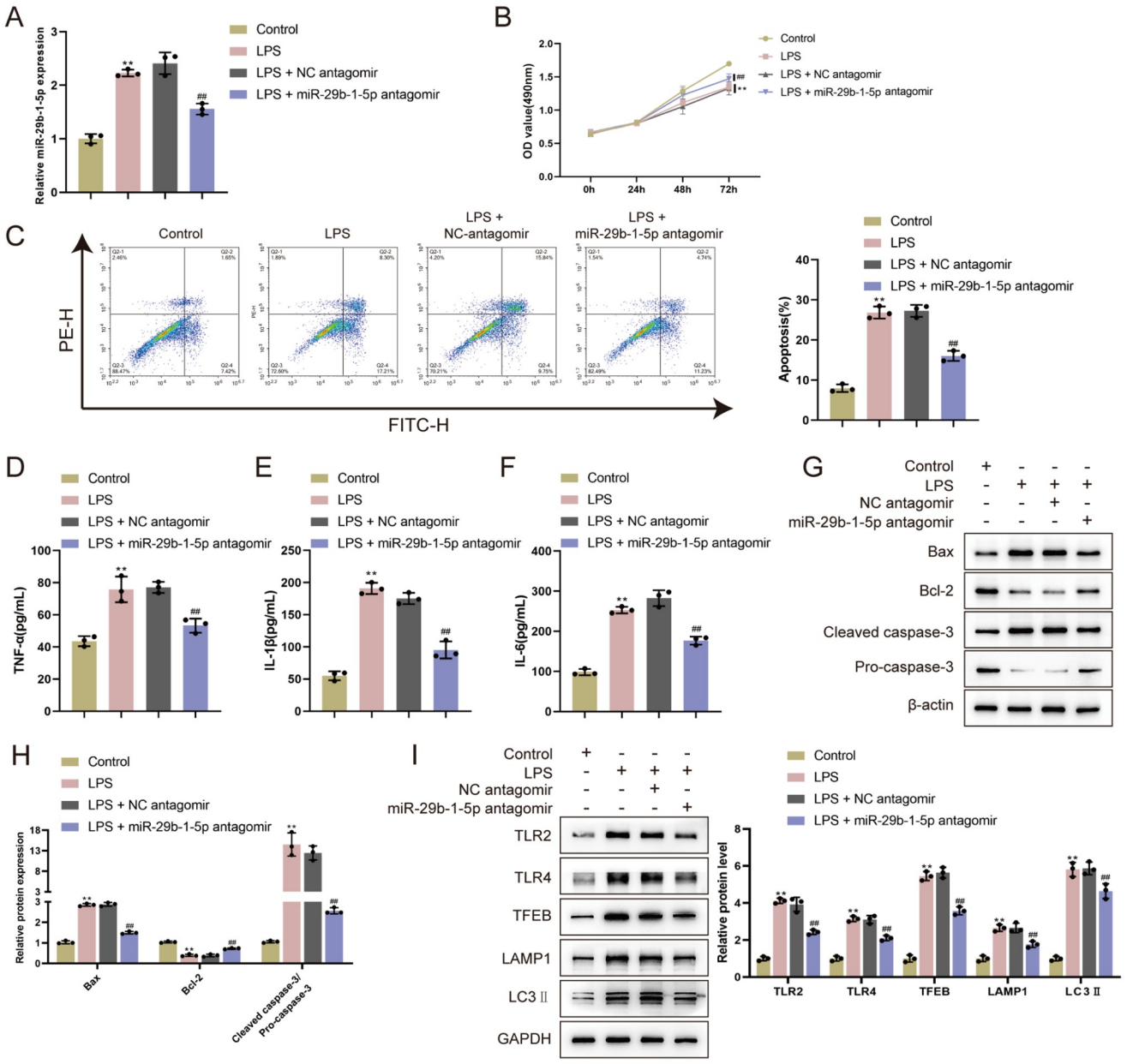

Figure 4. Inhibition of miR-29b-1-5p ameliorates LPS-induced cardiomyocyte dysfunction in mice *in vitro* (A) Twenty-four hours after transfecting HL-1 cells with the NC or miR-29b-1-5p antagomir, LPS (1 μg/mL) stimulation was applied for another 24 h, and miR-29b-1-5p expression was validated in each group by qRT-PCR. (B) After LPS treatment for 0, 24, 48, or 72 h, MTT assay was performed to examine the viability of the HL-1 cells. (C) Flow cytometry was used to evaluate apoptosis in HL-1 cells. (D–F) TNF-α, IL-1β, and IL-6 levels in HL-1 cell supernatants were measured by enzyme-linked immunosorbent assay (ELISA). (G–I) Western blot analysis was used to measure Bax, Bcl-2, cleaved caspase-3, pro-caspase-3, TLR2, TLR4, TFEB, LAMP1 and LC3II protein levels in HL-1 cells. $n = 3$. **$P < 0.01$ vs the control group; ##$P < 0.01$ vs the LPS + NC antagomir group.

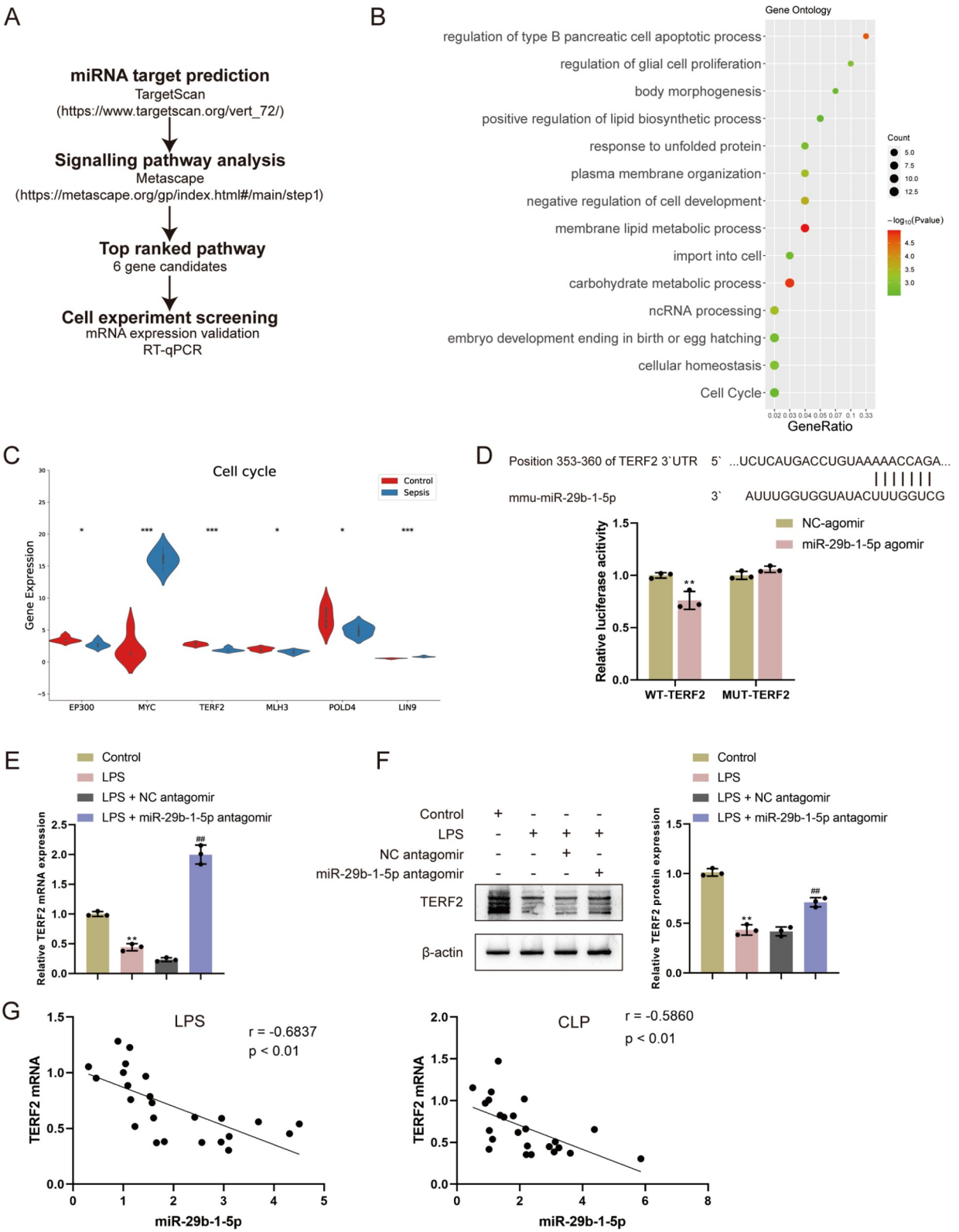

Figure 5. TERF2 is a downstream target of miR-29b-1-5p, and miR-29b-1-5p can target and inhibit TERF2 (A) Schematic diagram of miR-29b-1-5p target gene screening. (B) Metascape analysis of miR-29b-1-5p target gene function. (C) GSE185754 microarray analysis of miR-29b-1-5p target gene expression. (D) The ability of the predicted miR-29b-1-5p to target TERF2 was verified by dual-luciferase reporter gene assay. (E) qRT-PCR and (F) western blot analysis showing TERF2 mRNA and protein expression levels in response to LPS and miR-29b-1-5p antagomir transfection in HL-1 cells. (G) Correlation analysis between miR-29b-1-5p and TERF2 in the myocardial tissues of the LPS-treated mice and CLP-treated mice. $^{*}P<0.05$, $^{**}P<0.01$, $^{***}P<0.001$ vs the control group; $^{\#\#}P<0.01$ vs the LPS + NC antagomir group.

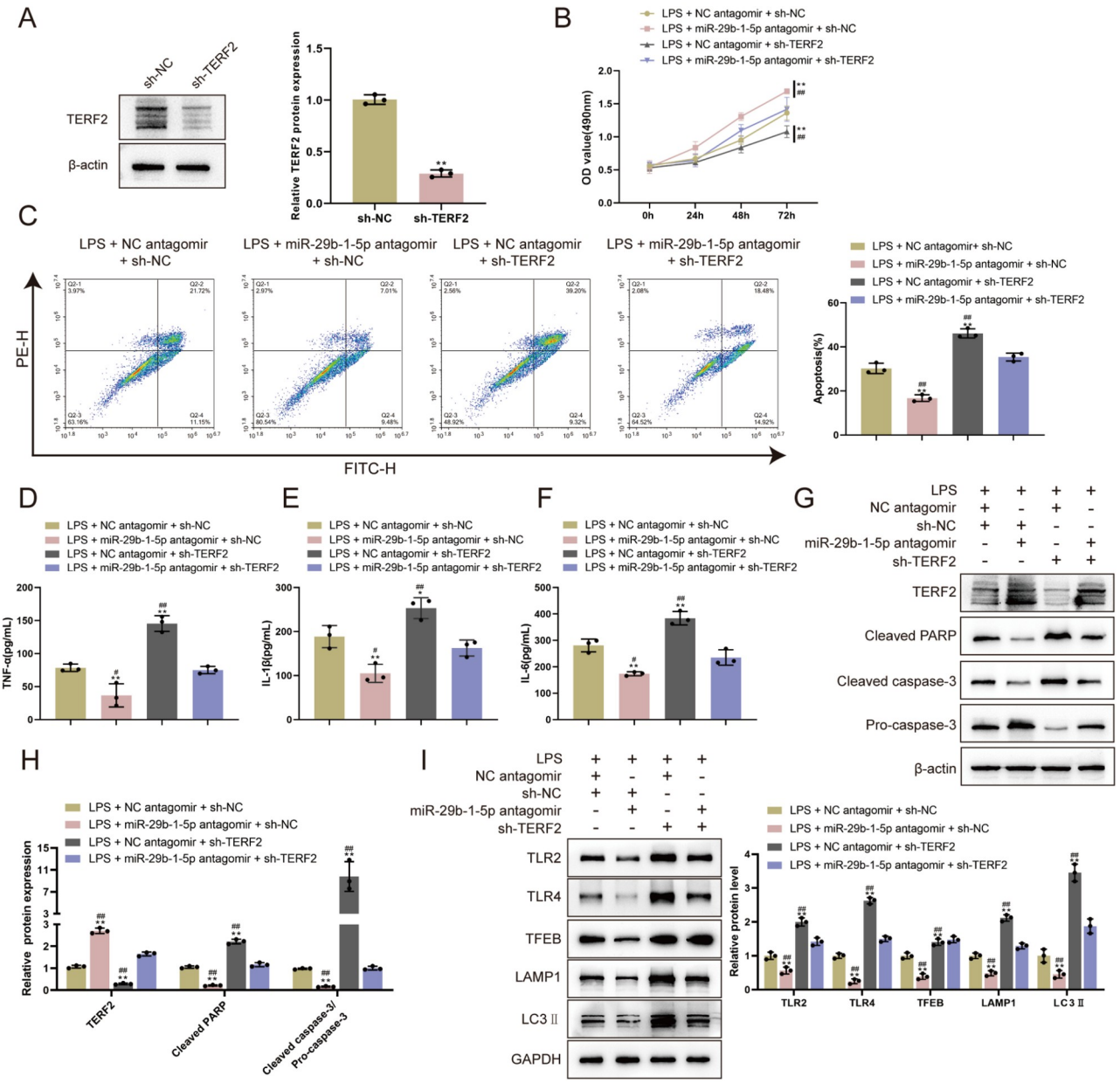

Figure 6. Silencing of *TERF2* partially reverses the ameliorative effect of miR-29b-1-5p inhibition on LPS-induced cardiomyocyte apoptosis and inflammation (A) HL-1 cells were transfected with sh-TERF2 or sh-NC vector. Forty-eight hours later, HL-1 cells were collected to detect the protein expression of TERF2. (B–I) HL-1 cells were transfected with sh-TERF2 or the miR-29b-1-5p antagomir for 24 h, followed by stimulation with LPS. MTT assay was performed to examine HL-1 cell viability (B). Flow cytometry was performed to evaluate HL-1 cell apoptosis (C). ELISA was also conducted to evaluate TNF-α, IL-1β, and IL-6 levels in HL-1 cells (D–F). Western blot analysis was conducted to determine the protein levels of TERF2, cleaved PARP, cleaved caspase-3, pro-caspase-3, TLR2, TLR4, TFEB, LAMP1 and LC3II in HL-1 cells (G–I). $^{**}P < 0.01$ vs LPS + NC antagomir + sh-NC; $^{\#}P < 0.05$, $^{\#\#}P < 0.01$ vs LPS + miR-29b-1-5p antagomir + sh-TERF2.

Sepsis-induced cardiac dysfunction is usually associated with reduced EF and FS, increased cardiomyocyte apoptosis, and enhanced inflammatory response [40]. Previous studies have reported that sepsis-induced myocardial injury and inflammation usually exhibit increased expressions of factors such as α-SMA in myocardial tissue and cTnI, TNF-α, IL-1β, and IL-6 in serum [12,41]. The LPS and CLP surgical models are general strategies for comprehending the process of sepsis-related myocardial dysfunction [42]. Numerous previous studies have shown that microRNAs play different roles in septic myocardial dysfunction. MiR-193-3p and miR-125b mitigate myocardial injury in septic mice by targeting the STAT3/HMGB1 axis [43,44]. However, miR-377 increases inflammation and cardiomyocyte hypertrophy in septic mice [45]. Here, the effects of miR-29b-1-5p on septic myocardial dysfunction were explored for the first time by constructing LPS and CLP models. miR-29b-1-5p expression was elevated in cardiac tissues from the LPS and CLP models. miR-29b-1-5p antagonists significantly improved the symptoms of septic myocardial injury, including increasing mouse survival, increasing cardiac function, decreasing α-SMA expression in myocardial tissue, decreasing

serum levels of cTnI, TNF-α, IL-1β, and IL-6, and alleviating myocardial tissue injury and fibrosis. Similar results were obtained when miR-29b-1-5p was inhibited in the LPS-induced cardiomyocyte model, which led to increased cardiomyocyte proliferation and inhibited apoptosis and inflammatory factor production. These data imply that the inhibition of miR-29b-1-5p protects against myocardial dysfunction induced by sepsis.

The downstream mechanisms of miR-29b-1-5p were further explored after confirming that elevated miR-29b-1-5p could contribute to the progression of myocardial injury in sepsis. miRNAs mostly regulate physiological effects in plants and animals by suppressing target mRNA expression [46], and miR-29b-1-5p is upregulated in septic myocardial disorder models. Therefore, the downstream target genes repressed by miR-29b-1-5p were further investigated via bioinformatics. Four downregulated target genes (*TERF2*, *Pold4*, *MLH3*, and *Ep300*) were identified. Analysis of TERF2 expression in LPS-induced cardiomyocytes showed that TERF2 expression was most significantly altered. TERF2 is a widely expressed protein that can bind directly to double telomeric repeat sequences in tandem arrays and is involved in the protection of telomere structure and chromosome ends [47]. Inhibition of TERF2 was previously reported to induce growth arrest and apoptosis in melanoma [48], laryngeal cancer [48,49], colorectal cancer [47], and other cancer cells. In addition, mutations in the TERF2 protein can cause persistent inflammation in vascular disease in atherosclerotic mice [50]. miRNAs mediate translation through partial base pairing to complementary sequences in the 3′UTR of target mRNAs [51]. Dual luciferase reporter gene assays verified that miR-29b-1-5p was able to bind to the 3′UTR of TERF2 and that miR-29b-1-5p negatively regulated TERF2 expression. Therefore, *TERF2* was considered a downstream target gene of miR-29b-1-5p. The inhibition of TERF2 expression in LPS-induced cardiomyocytes via functional reversion experiments showed that silencing of *TERF2* reversed the miR-29b-1-5p antagomir-induced upregulation of TERF2 expression, subsequently inhibited cell proliferation, promoted apoptosis and inflammatory cytokine expression, and partially abrogated the protective effect of the miR-29b-1-5p antagomir on septic cardiomyocyte injury. However, in addition to *TERF2*, several genes have also been reported to be regulated in a targeted manner by miR-29b-1-5p. In oral squamous cell carcinoma, miR-29b-1-5p targets cadherin 1 to promote EMT [52]. In gastric cancer, miR-29b-1-5p inhibits the expression of the PH domain and leucine-rich repeat protein phosphatase 1 (PHLPP1) to promote cell growth [53]. In septic mice, PHLPP1 could countermodulate the STAT1-mediated inflammatory pathway [54]. Cadherin 1 is reduced in a sepsis-induced acute kidney injury cell model [55]. However, further studies are needed to determine whether these genes are involved in the activity of miR-29b-1-5p in sepsis.

A number of studies have shown that sepsis can cause autophagy to occur in the heart and other organs and that autophagy changes dynamically throughout sepsis [56]. During autophagy, depletion of TERF2 promotes autophagy [57]. Lachettini *et al.* [58] reported that *TERF2* knockdown induces autophagy by sequestering HMGB1 into the nucleus, where it exerts its pro-autophagic effect when it is shuttled from the nucleus to the cytosol [59]. Moreover, inhibition of TERF2 leads to autophagic death, and apoptosis has also been proven to occur in gastric cancer [60]. Most current studies suggested that the induction of autophagy in sepsis can ameliorate sepsis-induced myocardial damage [30,61]. However, in the present study, we found that the miR-29b-1-5p antagomir had a cardioprotective effect on sepsis but inhibited LPS- or CLP-induced autophagy-lysosomal pathway activation. Similarly, Zhao *et al.* [62] confirmed that the reduction in the number of autophagosomes and the reduction in the expression of the lysosome marker LAMP1 are associated with the protective effect of ulinastatin in LPS-induced sepsis. The discrepancy in the role of cardiac autophagy in sepsis may be associated with the severity of sepsis, drug specificity, and difference in the timing of delivery [63].

In conclusion, this study demonstrated for the first time that inhibition of miR-29b-1-5p ameliorates septic myocardial injury. Mechanistically, inhibition of miR-29b-1-5p upregulates TERF2 expression, which in turn inhibits sepsis-induced myocardial tissue injury, inflammation, and cardiomyocyte apoptosis. Our findings indicate that miR-29b-1-5p may be a promising therapeutic target for septic myocardial injury.

Supplementary Data

Supplementary data is available at *Acta Biochimica et Biophysica Sinica* online.

Funding

This work was supported by the grants from the National Natural Science Foundation of China (No. 81971819 and No. 82204986) and the Scientific Research Plan Project of Hunan Provincial Health Commission (No. D202304117248).

Conflict of Interest

The authors declare that they have no conflict of interest.

References

1. Hamaguchi M, Wu HN, Tanaka M, Tsuda N, Tantengco OAG, Matsushima T, Nakao T, *et al.* A case series of the dynamics of lipid mediators in patients with sepsis. *Acute Med Surg* 2019, 6: 413–418
2. Dimopoulos G, Rovina N, Patrani M, Antoniadou E, Konstantonis D, Vryza K, Vlachogianni G, *et al.* Past history of stage I/II solid tumor malignancy impacts considerably on sepsis mortality: a propensity score matching analysis from the hellenic sepsis study group. *BMC Infect Dis* 2019, 19: 831
3. Romero-Bermejo FJ, Ruiz-Bailen M, Gil-Cebrian J, Huertos-Ranchal MJ. Sepsis-induced cardiomyopathy. *Curr Cardiol Rev* 2011, 7: 163–183
4. Hochstadt A, Meroz Y, Landesberg G. Myocardial dysfunction in severe sepsis and septic shock: more questions than answers? *J Cardiothoracic Vascular Anesth* 2011, 25: 526–535
5. Kakihana Y, Ito T, Nakahara M, Yamaguchi K, Yasuda T. Sepsis-induced myocardial dysfunction: pathophysiology and management. *J Intensive Care* 2016, 4: 22
6. Fang X, Ardehali H, Min J, Wang F. The molecular and metabolic landscape of iron and ferroptosis in cardiovascular disease. *Nat Rev Cardiol* 2023, 20: 7–23
7. Meng S, Zhou H, Feng Z, Xu Z, Tang Y, Li P, Wu M. CircRNA: functions and properties of a novel potential biomarker for cancer. *Mol Cancer* 2017, 16: 94
8. Zhelankin AV, Vasiliev SV, Stonogina DA, Babalyan KA, Sharova EI, Doludin YV, Shchekochikhin DY, *et al.* Elevated plasma levels of circulating extracellular miR-320a-3p in patients with paroxysmal atrial fibrillation. *Int J Mol Sci* 2020, 21: 3485
9. Wang L, Wang HC, Chen C, Zeng J, Wang Q, Zheng L, Yu HD. Differential expression of plasma miR-146a in sepsis patients compared with non-

sepsis-SIRS patients. *Exp Ther Med* 2013, 5: 1101–1104
10. Ailawadi S, Wang X, Gu H, Fan GC. Pathologic function and therapeutic potential of exosomes in cardiovascular disease. *Biochim Biophys Acta Mol Basis Dis* 2015, 1852: 1–11
11. Halushka PV, Goodwin AJ, Halushka MK. Opportunities for microRNAs in the crowded field of cardiovascular biomarkers. *Annu Rev Pathol Mech Dis* 2019, 14: 211–238
12. Wu M, Huang Z, Huang W, Lin M, Liu W, Liu K, Li C. microRNA-124-3p attenuates myocardial injury in sepsis via modulating SP1/HDAC4/HIF-1α axis. *Cell Death Discov* 2022, 8: 40
13. Long X, Huang Y, He J, Zhang X, Zhou Y, Wei Y, Tang Y, ***et al.*** Upregulation of miR-335 exerts protective effects against sepsis-induced myocardial injury. *Mol Med Rep* 2021, 24: 806
14. Kulasingam V, Diamandis EP. Strategies for discovering novel cancer biomarkers through utilization of emerging technologies. *Nat Rev Clin Oncol* 2008, 5: 588–599
15. Zhang T, Guo J, Gu J, Wang Z, Wang G, Li H, Wang J. Identifying the key genes and microRNAs in colorectal cancer liver metastasis by bioinformatics analysis and *in vitro* experiments. *Oncol Rep* 2019, 41: 279–291
16. Fu Q, Yu W, Fu S, Xu Z, Zhang S. MicroRNA-449c-5p alleviates lipopolysaccharide-induced HUVECs injury via inhibiting the activation NF-κB signaling pathway by TAK1. *Mol Immunol* 2022, 146: 18–26
17. Zou HX, Hu T, Zhao JY, Qiu BQ, Zou CC, Xu QR, Liu JC, ***et al.*** Exploring dysregulated ferroptosis-related genes in septic myocardial injury based on human heart transcriptomes: evidence and new insights. *J Inflamm Res* 2023, 16: 995–1015
18. Wang L, Li Y, Wang X, Wang P, Essandoh K, Cui S, Huang W, ***et al.*** GDF3 protects mice against sepsis-induced cardiac dysfunction and mortality by suppression of macrophage pro-inflammatory phenotype. *Cells* 2020, 9: 120
19. Krützfeldt J, Rajewsky N, Braich R, Rajeev KG, Tuschl T, Manoharan M, Stoffel M. Silencing of microRNAs *in vivo* with 'antagomirs'. *Nature* 2005, 438: 685–689
20. Guo C, Ye FX, Jian YH, Liu CH, Tu ZH, Yang DP. MicroRNA-214-5p aggravates sepsis-related acute kidney injury in mice. *Drug Dev Res* 2022, 83: 339–350
21. Lin Y, Hu J, Chen J, Chen S, Cai Y, Lin C. MiR-155 protects against sepsis-induced cardiomyocyte apoptosis via activation of NO/cGMP signaling pathway by eNOS. *Trop J Pharm Res* 2022, 21: 1851–1858
22. Ruan W, Ji X, Qin Y, Zhang X, Wan X, Zhu C, Lv C, ***et al.*** Harmine alleviated sepsis-induced cardiac dysfunction by modulating macrophage polarization via the STAT/MAPK/NF-κB pathway. *Front Cell Dev Biol* 2021, 9: 792257
23. Li Q, Li L, Fei X, Zhang Y, Qi C, Hua S, Gong F, ***et al.*** Inhibition of autophagy with 3-methyladenine is protective in a lethal model of murine endotoxemia and polymicrobial sepsis. *Innate Immun* 2018, 24: 231–239
24. Zeng N, Jian Z, Xu J, Zheng S, Fan Y, Xiao F. DLK1 overexpression improves sepsis-induced cardiac dysfunction and fibrosis in mice through the TGF-β1/Smad3 signaling pathway and MMPs. *J Mol Histol* 2023, 54: 655–664
25. Ali MIM, Imbaby S, Arafat HEK, Maher SA, Kolieb E, Ali SM. Cardioprotective and renoprotective effects of venlafaxine on cisplatin-induced cardiotoxicity and nephrotoxicity in rats. *Life Sci* 2023, 320: 121561
26. Imbaby S, Elkholy SE, Faisal S, Abdelmaogood AKK, Mehana AE, Mansour BSA, Abd El-moneam SM, ***et al.*** The GSTP1/MAPKs/BIM/SMAC modulatory actions of nitazoxanide: bioinformatics and experimental evidence in subcutaneous solid Ehrlich carcinoma-inoculated mice. *Life Sci* 2023, 319: 121496
27. Meng XL, Yu MM, Liu YC, Gao YL, Chen XS, Shou ST, Chai YF. Rutin inhibits cardiac apoptosis and prevents sepsis-induced cardiomyopathy. *Front Physiol* 2022, 13: 834077
28. Ali SM, Kolieb E, Imbaby S, Hagras AM, Korayem Arafat HE, Kamel EM, Abdelshakour MA, ***et al.*** Acute toxic effects of new synthetic cannabinoid on brain: neurobehavioral and histological: preclinical studies. *Chem-Biol Interact* 2023, 370: 110306
29. Imbaby S, Hattori Y. Stattic ameliorates the cecal ligation and puncture-induced cardiac injury in septic mice via IL-6-gp130-STAT3 signaling pathway. *Life Sci* 2023, 330: 122008
30. Zou X, Xu J, Yao S, Li J, Yang Y, Yang L. Endoplasmic reticulum stress-mediated autophagy protects against lipopolysaccharide-induced apoptosis in HL-1 cardiomyocytes. *Exp Physiol* 2014, 99: 1348–1358
31. Livak KJ, Schmittgen TD. Analysis of relative gene expression data using real-time quantitative PCR and the 2−ΔΔCT method. *Methods* 2001, 25: 402–408
32. Eslami A, Lujan J. Western blotting: sample preparation to detection. *J Vis Exp* 2010, 14: 2359
33. Zhou Y, Song Y, Shaikh Z, Li H, Zhang H, Caudle Y, Zheng S, ***et al.*** MicroRNA-155 attenuates late sepsis-induced cardiac dysfunction through JNK and β-arrestin 2. *Oncotarget* 2017, 8: 47317–47329
34. Wang H, Bei Y, Huang P, Zhou Q, Shi J, Sun Q, Zhong J, ***et al.*** Inhibition of miR-155 protects against LPS-induced cardiac dysfunction and apoptosis in mice. *Mol Ther Nucleic Acids* 2016, 5: e374
35. Liu X, Zheng X, Lu Y, Chen Q, Zheng J, Zhou H. TFEB dependent autophagy-lysosomal pathway: an emerging pharmacological target in sepsis. *Front Pharmacol* 2021, 12: 794298
36. Toscano MG, Ganea D, Gamero AM. Cecal ligation puncture procedure. *J Vis Exp* 2011, 7: 2860
37. Rudd KE, Johnson SC, Agesa KM, Shackelford KA, Tsoi D, Kievlan DR, Colombara DV, ***et al.*** Global, regional, and national sepsis incidence and mortality, 1990–2017: analysis for the Global Burden of Disease Study. *Lancet* 2020, 395: 200–211
38. Xin Y, Tang L, Chen J, Chen D, Wen W, Han F. Inhibition of miR-101-3p protects against sepsis-induced myocardial injury by inhibiting MAPK and NF-κB pathway activation via the upregulation of DUSP1. *Int J Mol Med* 2021, 47: 20
39. Long B, Li N, Xu XX, Li XX, Xu XJ, Guo D, Zhang D, ***et al.*** Long noncoding RNA FTX regulates cardiomyocyte apoptosis by targeting miR-29b-1-5p and Bcl2l2. *Biochem Biophys Res Commun* 2018, 495: 312–318
40. Li Z, Zhu H, Liu C, Wang Y, Wang D, Liu H, Cao W, ***et al.*** GSK-3β inhibition protects the rat heart from the lipopolysaccharide-induced inflammation injury via suppressing FOXO3A activity. *J Cell Mol Medi* 2019, 23: 7796–7809
41. Zhang L, Jian X, Yu J, Yu J. Pterostilbene interferes with lipopolysaccharide-induced myocardial injury through oxidative stress and inflammasome pathways. *Front Physiol* 2022, 13: 862187
42. Li Z, Meng Y, Liu C, Liu H, Cao W, Tong C, Lu M, ***et al.*** Kcnh2 mediates FAK/AKT-FOXO3A pathway to attenuate sepsis-induced cardiac dysfunction. *Cell Prolif* 2021, 54: e12962
43. Pan J, Alexan B, Dennis D, Bettina C, Christoph LIM, Tang Y. microRNA-193-3p attenuates myocardial injury of mice with sepsis via STAT3/HMGB1 axis. *J Transl Med* 2021, 19: 386
44. Yu Y, Ou-Yang WX, Zhang H, Jiang T, Tang L, Tan YF, Luo HY, ***et al.*** MiR-125b enhances autophagic flux to improve septic cardiomyopathy via targeting STAT3/HMGB1. *Exp Cell Res* 2021, 409: 112842
45. Wang S, Wang G, Dong L, Liu X, Pan W, Han J, Lu Y. The overexpression

of miR-377 aggravates sepsis-induced myocardial hypertrophy by binding to Rcan2 and mediating CaN activity. *Oxid Med Cell Longev* 2022, 2022: 6659183
46. Bartel DP. MicroRNAs: genomics, biogenesis, mechanism, and function. *Cell* 2004, 116: 281–297
47. Dong W, Shen R, Wang Q, Gao Y, Qi X, Jiang H, Yao J, ***et al.*** Sp1 upregulates expression of TRF2 and TRF2 inhibition reduces tumorigenesis in human colorectal carcinoma cells. *Cancer Biol Ther* 2009, 8: 2165–2173
48. Biroccio A, Rizzo A, Elli R, Koering CE, Belleville A, Benassi B, Leonetti C, ***et al.*** TRF2 inhibition triggers apoptosis and reduces tumourigenicity of human melanoma cells. *Eur J Cancer* 2006, 42: 1881–1888
49. Jiao L, Xu Y, Tao Z. Experiment studies on growth and proliferation of Hep-2 cells by silence of TRF2 gene. *Lin Chung Er Bi Yan Hou Tou Jing Wai Ke Za Zhi* 2010, 24: 1131–1135
50. Uryga AK, Grootaert MOJ, Garrido AM, Oc S, Foote K, Chappell J, Finigan A, ***et al.*** Telomere damage promotes vascular smooth muscle cell senescence and immune cell recruitment after vessel injury. *Commun Biol* 2021, 4: 611
51. Gu S, Jin L, Zhang F, Sarnow P, Kay MA. Biological basis for restriction of microRNA targets to the 3′ untranslated region in mammalian mRNAs. *Nat Struct Mol Biol* 2009, 16: 144–150
52. Kurihara-Shimomura M, Sasahira T, Shimomura H, Nakashima C, Kirita T. The oncogenic activity of miR-29b-1-5p induces the epithelial-mesenchymal transition in oral squamous cell carcinoma. *J Clin Med* 2019, 8: 273
53. Xu F, Chen M, Chen H, Wu N, Qi Q, Jiang X, Fang D, ***et al.*** The curcumin analog Da0324 inhibits the proliferation of gastric cancer cells via HOTAIRM1/miR-29b-1-5p/PHLPP1 axis. *J Cancer* 2022, 13: 2644–2655
54. Cohen Katsenelson K, Stender JD, Kawashima AT, Lordén G, Uchiyama S, Nizet V, Glass CK, ***et al.*** PHLPP1 counter-regulates STAT1-mediated inflammatory signaling. *Elife* 2019, 8: e48609
55. Sun J, Wei S, Zhang Y, Li J. Protective effects of astragalus polysaccharide on sepsis-induced acute kidney injury. *Anal Cell Pathol* 2021, 2021: 7178253
56. Yin X, Xin H, Mao S, Wu G, Guo L. The role of autophagy in sepsis: protection and injury to organs. *Front Physiol* 2019, 10: 1071
57. Zlotorynski E. Telomere crisis activates autophagic death. *Nat Rev Mol Cell Biol* 2019, 20: 133
58. Iachettini S, Ciccarone F, Maresca C, D'Angelo C, Petti E, Di Vito S, Ciriolo MR, ***et al.*** The telomeric protein TERF2/TRF2 impairs HMGB1-driven autophagy. *Autophagy* 2023, 19: 1479–1490
59. Chen R, Kang R, Tang D. The mechanism of HMGB1 secretion and release. *Exp Mol Med* 2022, 54: 91–102
60. Yang Q, Nie Z, Zhu Y, Hao M, Liu S, Ding X, Wang F, ***et al.*** Inhibition of TRF2 leads to ferroptosis, autophagic death, and apoptosis by causing telomere dysfunction. *Oxid Med Cell Longev* 2023, 2023: 6897268
61. Han W, Wang H, Su L, Long Y, Cui N, Liu D. Inhibition of the mTOR pathway exerts cardioprotective effects partly through autophagy in CLP rats. *Mediators Inflamm* 2018, 2018: 1–9
62. Zhao P, Zhang L, Gao L, Ding Q, Yang Q, Kuai J. Ulinastatin attenuates lipopolysaccharide-induced cardiac dysfunction by inhibiting inflammation and regulating autophagy. *Exp Ther Med* 2020, 20: 1064–1072
63. Sun Y, Cai Y, Zang QS. Cardiac autophagy in sepsis. *Cells* 2019, 8: 141